International Journal of Biological Macromolecules 121 (2019) 524–535

Contents lists available at ScienceDirect

International Journal of Biological Macromolecules

journal homepage: http://www.elsevier.com/locate/ijbiomac

# Production and characterization of electrospun silk fibroin based asymmetric membranes for wound dressing applications

Sónia P. Miguel [a], Déborah Simões [a], André F. Moreira [a], Rosa S. Sequeira [a], Ilídio J. Correia [a,b,*]

[a] CICS-UBI – Centro de Investigação em Ciências da Saúde, Universidade da Beira Interior, Av. Infante D. Henrique, 6200-506 Covilhã, Portugal
[b] CIEPQPF – Departamento de Engenharia Química, Universidade de Coimbra, Rua Sílvio Lima, 3030-790 Coimbra, Portugal

ARTICLE INFO

*Article history:*
Received 15 September 2018
Received in revised form 10 October 2018
Accepted 10 October 2018
Available online 11 October 2018

*Keywords:*
Electrospun asymmetric membranes
Silk fibroin
Thymol

ABSTRACT

Nowadays, wound dressings with improved properties are under development and among them, asymmetric membranes have gained an increasing interest due to their two-layered structure that mimic both the epidermis and dermis layers of the skin. Herein, a new asymmetric membrane was produced using the electrospinning technique. The top layer was produced with silk fibroin (SF) and poly(caprolactone) to reproduce the dense nature and waterproof ability of the epidermis. On the other hand, the dermis-like bottom layer was manufactured with SF and hyaluronic acid loaded with an herbal drug (thymol (THY)). All the data gathered showed that the produced electrospun asymmetric membrane exhibited the porosity, wettability, and mechanical properties suitable for the healing process. Further, the *in vitro* data also demonstrated that the human fibroblast is able to adhere and spread at the membranes' surface, thus confirming their biocompatibility. Moreover, the incorporation of THY into the bottom layer of the membrane, improved its antioxidant and antibacterial properties. Overall, the obtained results demonstrate the appropriateness of the produced membrane for wound healing applications.



## 1. Introduction

A wound results from a sharp injury, that affects the skin' structure and disrupts the cells' crosstalk interactions and functions across the skin layers [1]. Skin injuries can represent a severe health risk to the human body since skin' functions such as thermal insulation, body fluid retention and protection from external threats can be hindered [2]. To avoid further complications, after a skin injury occurs, an immediate covering of the wound is required to protect the underlying tissues from hazard agents as well as prevent fluid loss [3].

Up to now, in the clinic, the traditional wound dressings (*e.g.* gauzes, bandages, and creams) and skin grafts have been the most used therapeutic approaches, and they act as temporary barriers. However, most of them are expensive, require frequent replacement, and are not able to fully re-establish skin structure and functions [4]. Therefore, the development of new therapeutic strategies or methodologies to assist the wound healing mechanism is extremely important. Among the different wound dressings under development, the nanofibrous membranes have received an increasing attention due to their intrinsic properties, such as high surface-to-volume ratio, interconnected pores that are compatible with cell penetration and nutrient exchange, as well as the potential to promote the hemostasis phase and wound exudate absorption [4,5]. In addition, the nanofibers are able to mimic the structure of the proteins (*e.g.* laminin and collagen) found in the natural extracellular matrix (ECM) [5].

Different techniques (self-assembly, dry/wet phase separation, electrospinning, and $scCO_2$-induced phase inversion) have been used to produce nanofibrous membranes. The electrospinning technique is one of the most explored to produce nanofibers due to its simplicity, efficacy, reproducibility and versatility. Recently, this methodology has also been employed for the manufacture of Nanofibrous Asymmetric Membranes [5,6]. The main feature of this type of wound dressing is their two-layered structure that is able to mimic both skin layers (epidermis and dermis). In general, an asymmetric membrane displays (i) a dense and waterproof top layer that confers protection to the wound site in a similar way to the epidermis layer and (ii) a porous bottom layer that reproduces the dermis structure [6,7].

Herein, an electrospun asymmetric membrane (EAM) composed of two interconnected layers was produced for enhancing the healing process. The top layer was composed of SF and poly(caprolactone) (PCL), while the bottom layer was produced by using a blend of SF with hyaluronic acid (HA). SF is a fibrous protein synthesized by a variety of insects including silkworm and presents excellent biocompatibility, good water vapor permeability, biodegradability, mechanical strength, and minimal inflammatory reaction [8]. In turn, PCL is a hydrophobic synthetic polymer that exhibits a high mechanical strength. The

* Corresponding author at: CICS-UBI - Centro de Investigação em Ciências da Saúde, Universidade da Beira Interior, Avenida Infante D. Henrique, 6200-506 Covilhã, Portugal.
*E-mail address:* icorreia@ubi.pt (I.J. Correia).

https://doi.org/10.1016/j.ijbiomac.2018.10.041
0141-8130/

combination of SF with PCL was used to produce a layer that presents epidermis-like properties such as the hydrophobic character, waterproof ability and mechanical resistance [6]. On the other side, the HA was selected since it is a hydrophilic and polyanionic polymer that can be found in connective tissues (*e.g.* skin, ligament, cartilage, blood vessels) and provides a high capacity of hydration, water-sorption and water retention, as well as allows cell attachment, migration, and proliferation [5,9]. Therefore, the production of a porous bottom layer composed of SF/HA combination should result in a dermis-like structure, capable of absorbing the wound exudate as well as promote the cell adhesion and proliferation. Furthermore, to confer antimicrobial activity to the bottom layer, Thymol (THY), an herbal drug, was loaded into the nanofibers mesh [10]. THY is the major component of the essential oils extracted from *Lippia gracilis* and it exhibits various biological effects such as antimicrobial, antioxidant, antinociceptive, local anesthetic, and anti-inflammatory [11]. Up to now, THY has been applied as an active antiseptic ingredient in some toothpastes, such as Euthymol® (Johnson & Johnson's). Further, when comparing to other essential oils, such as carvacrol, THY shows an increased antioxidant potential [12]. However, the addition of THY into electrospun asymmetric membranes and its impact on the biological properties of the wound dressing materials is poorly explored in the literature.

## 2. Methods

### 2.1. Production of the electrospun asymmetric membrane

The production of the **EAM** membrane was performed using a conventional electrospinning apparatus, comprised of high voltage source (Spellman CZE1000R, 0–30 kV) (obtained from Spellman, Corporate Headquarters USA) a precision syringe pump (KDS-100) (acquired from Sigma-Aldrich, Sintra, Portugal), a plastic syringe with a stainless-steel needle (21 Gauge), and an aluminium disk connected to a copper collector. The top layer (**SF_PCL**) of the membrane was produced by using a blend composed of SF (10% w/v) and PCL (10% w/v) dissolved in a solution of Formic acid (FA) (98% v/v) and Trifluoroethanol (TFE) (80% v/v) at 2:1 volume ratio. Then, this solution was placed in the syringe and electrospun at a constant flow rate of 1.0 mL/h, using a working distance of 10–12 cm and an applied voltage of 28 kV, until a thickness similar to the epidermis layer of the human skin (0.05–1.5 mm) was obtained. Posteriorly, the bottom layer (**SF_HA_THY**) was produced by combining the solutions of SF (10% w/v) in FA (98% v/v) and HA (20% w/v) in $H_2O$ at 2:1 volume ratio. Subsequently, THY at a concentration of 5 mg/mL and 2 mL of Polyethylene oxide (PEO) (8% w/v) were added to the blend. PEO was added to the blend to adjust its viscosity in order to improve its electrospinability. Afterwards, the polymeric solution was electrospun on top of the SF_PCL membrane at a constant flow rate of 2.3 mL/h, using a working distance of 12 cm and an applied voltage of 28 kV. The bottom layer without THY (**SF_HA**) was also produced for comparative purposes. In the same way, the electrospun of the bottom layer was performed until an obtained thickness value of 1.5–4 mm (dermis layer thickness).

To improve the water stability of SF, all membranes were treated with ethanol vapor (75%) at 25 °C, for 1 h and then dried under vacuum at room temperature (RT) for 2 h [13]. This procedure induces structural changes, through a crystallization process, being observed the transition from silk I (random coil) to silk II (β sheet) conformation. Afterwards, the membranes mechanical and physicochemical properties were evaluated (please see the supporting information for further details).

### 2.2. Evaluation of the encapsulation and loading efficiency of THY within the bottom layer of produced EAM

To evaluate the encapsulation and loading efficiency of THY, the uncrosslinked SF_HA and SF_HA_THY layers were subjected to total degradation, through their immersion in FA, during 1 h, under stirring. Then, the supernatant was recovered by centrifugation at 14,000 rpm for 10 min, and the absorbance was measured at 274 nm by using a Thermo Scientific Evolution 201 UV–vis spectrophotometer [10]. The THY concentration in the supernatant was determined using a standard absorbance curve (Fig. S2A) of THY at 274 nm ($y = 0.0202x + 2.153$, $R^2 = 0.9988$). The UV absorbance spectra of SF_HA and SF_HA_THY were also recorded for control purposes (Fig. S2B). The encapsulation efficiency (EE) and loading efficiency (LE) were determined using the following Eqs. (1) and (2):

$$EE\ (\%) = \frac{W_i - W_s}{W_i} \times 100 \quad (1)$$

$$LE\ (\%) = \frac{W_i - W_s}{Y} \times 100 \quad (2)$$

where $W_i$ is the total amount of THY added in SF_HA_THY membrane, $W_s$ is the amount of THY in the supernatant, and $Y$ is the total dry weight of SF_HA_THY membrane.

### 2.3. Analysis of the drug-release kinetics

The amount of THY released from the electrospun membranes was measured according to a method previously reported in the literature [10]. The electrospun membranes (with a total weight of 5 mg) were immersed in 2 mL of PBS at pH 5 or pH 8. The samples were then incubated at 37 °C under agitation (60 rpm) in an incubator shaker, to mimic the physiological conditions. At different timepoints, the samples were centrifugated and the supernatant (1 mL) absorbance was measured at 274 nm, using a Thermo Scientific Evolution 201 UV–vis spectrophotometer, to determine the amount of THY released. All experiments were performed in triplicate.

Further, the drug-release kinetics exhibited by the produced membranes were also characterized by using the Peppas-Korsmeyer Eq. (3) and Hixon-Crowell models Eq. (4):

$$\text{Peppas}-\text{Korsmeyer}: \frac{M_t}{M_\infty} = \text{Kt}^n \quad (3)$$

$$\text{Hixon}-\text{Crowell}: Q_0^{1/3} = Q_t^{1/3} - K_s t \quad (4)$$

where $M_t$ is the cumulative amount of drug released at time $t$, $M_\infty$ is the initial drug loading, $K$ is a constant characteristic of the drug-polymer system, and $n$ is the diffusion exponent, suggesting the nature of the release mechanism. $Q_t$ is the amount of drug dissolved in time t and $Q_0$ is the initial amount of drug in the solution.

### 2.4. Characterization of EAM biocompatibility

#### 2.4.1. Characterization of cell viability and proliferation when they are in contact with the produced membranes

The membranes' biocompatibility was evaluated using an MTS assay as recommended by the ISO 10993-5:2009 (Biological evaluation of medical devices- Part 5: Tests for *in vitro* cytotoxicity). Prior to cell seeding, membranes were placed into 96-well plates, occupying <10% of the well area, and then sterilized under UV irradiation (254 nm, ≈7 mW $cm^{-2}$) for 1 h. After, Normal Human Dermal Fibroblasts (NHDF) cells were seeded at a density of $10 \times 10^3$ cells per well and incubated at 37 °C, in an incubator with a 5% $CO_2$ humidified atmosphere. After 1, 3 or 7 days of incubation, the medium of each well was removed and replaced by a mixture of 100 μL of fresh culture medium and 20 μL of MTS/PMS (phenazine methosulfate) reagent solution and incubated for 4 h, at 37 °C, in a 5% $CO_2$ atmosphere. The absorbance of each sample ($n = 5$) was determined at 492 nm using a microplate reader (Biorad xMark microplate spectrophotometer). Cells incubated with ethanol (96%) were used as positive control ($K^+$), whereas cells incubated only with culture medium were used as a negative control ($K^-$).

### 2.5. Evaluation of the antimicrobial properties of the EAM

#### 2.5.1. Analysis of bacterial penetration through the top layer of EAM

*Staphylococcus aureus* (*S. aureus*) and *Pseudomonas aeruginosa* (*P. aeruginosa*), gram-positive and gram-negative bacteria respectively, were used to characterize the capacity of the membrane's top layer to avoid bacterial infiltration within their structure. To accomplish this, transwell systems (Corning Incorporated, New York, NY, USA) were modified with SF_PCL membrane or a filter paper (0.22 μm) (control group) to act as the interface between the upper and lower chamber. The SF_PCL membrane and the filter paper were inoculated with a bacterial suspension ($1 \times 10^8$ colony forming units (CFU)/mL), for 24 h, at 37 °C. Afterwards, the optical density (absorbance value at 600 nm) of the culture medium present in the lower chamber was measured and the number of colonies that crossed the SF_PCL membrane/filter paper were counted. In addition, the presence of microorganisms at the upper and bottom surfaces of the SF_PCL membrane or in the filter paper were investigated through SEM.

#### 2.5.2. Characterization of the antibacterial activity of the bottom layer of EAM

The bactericidal activity of the bottom layers of SF_HA and SF_HA_THY was also characterized using *S. aureus* and *P. aeruginosa*, as models. Briefly, 25–50 mg of each sample were added to 10 mL of LB broth, at pH 6.2, containing $1 \times 10^5$ CFU/mL of early mid-log phase bacteria culture and then incubated at 37 °C, for 24 h. After the incubation period, serial dilutions were prepared and 100 μL of bacterial samples were transferred into LB agar plates. Following overnight incubation at 37 °C, bacterial colonies were counted and expressed as CFU/mL. The bacterial growth inhibition was calculated through Eq. (5):

$$\textit{Antibacterial efficiency}\ (\%) = \frac{N_0 - N}{N_0} \times 100 \tag{5}$$

where $N_0$ and N each represent the bacteria number of control and experimental group, respectively.

Furthermore, a modified Kirby-Bauer technique was used to characterize the antimicrobial properties of the membranes. For this, circular membranes (n = 3) were placed on the surface of an agar plate seeded with *S. aureus* or *P. aeruginosa* ($1 \times 10^8$ CFU/mL) and incubated for 24 h, at 37 °C. After that, the inhibitory halos around the samples were photographed and the halo size determined with an image analysis software, ImageJ (Scion Corp., Frederick, MD). In addition, the biofilm formation at the surface of the membranes was also assessed through SEM analysis.

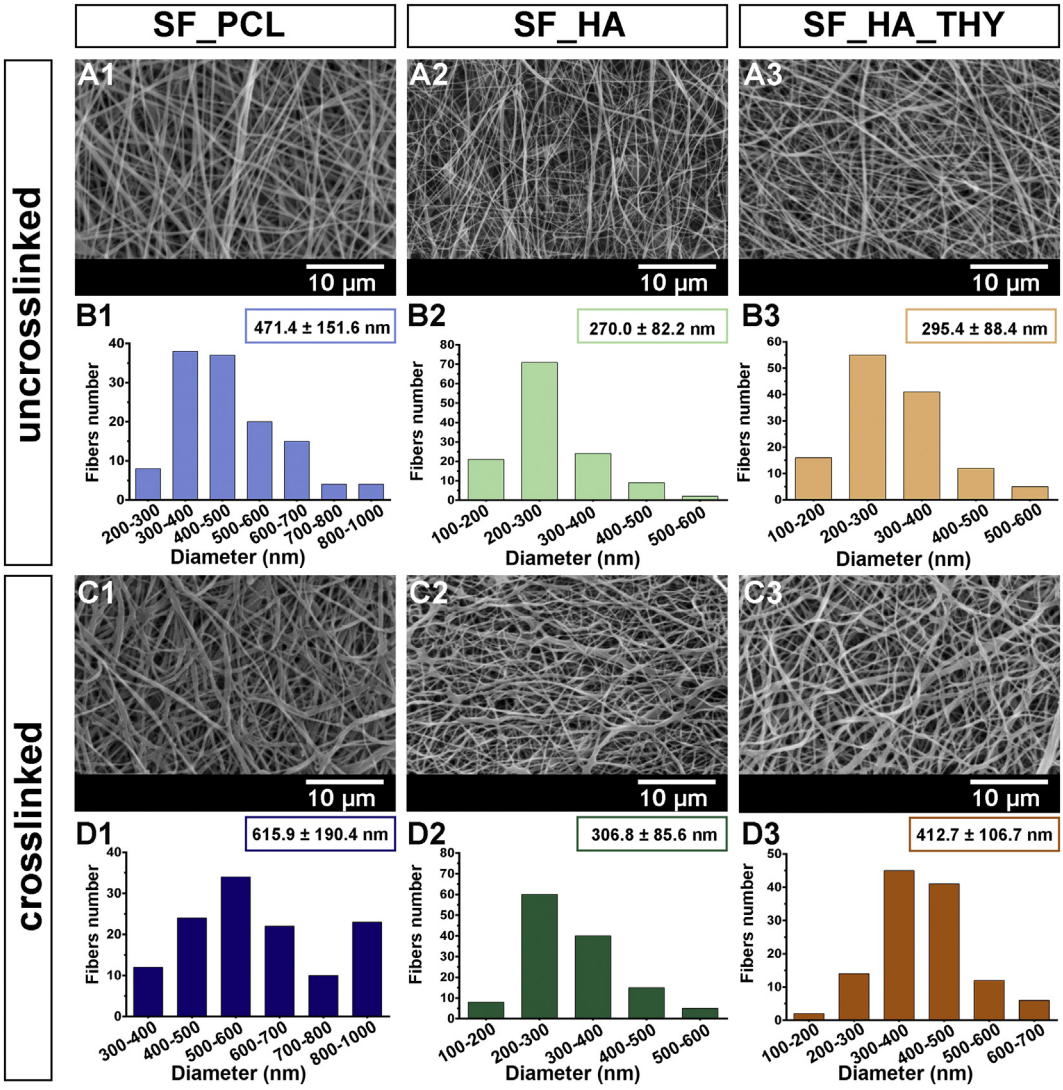


**Fig. 1.** Characterization of the SF_PCL, SF_HA, and SF_HA_THY nanofibrous layers morphological properties. SEM images of the top and bottom layers, before (A1–A3) and after the crosslinking process (C1–C3). Top and bottom layers nanofibers diameter distribution before and after crosslinking are presented in (B1–B3) and (D1–D3), respectively.

### 2.6. Statistical analysis

The statistical analysis of the obtained results was performed using one-way analysis of variance (ANOVA), with the Newman-Keuls *post hoc* test. A p value lower than 0.05 ($p < 0.05$) was considered statistically significant.

## 3. Results and discussion

### 3.1. Characterization of the morphology of the membranes

In recent years, asymmetric membranes have become the main target of different studies to develop wound dressings that can mimic the structure and functions of human skin [5,6]. In this study, an electrospinning technique was used to produce a novel asymmetric membrane based on a silk derived biopolymer enriched with a natural compound, THY. The dense top SF_PCL layer provides mechanical support, acts as a physical barrier to protect the wound from mechanical and chemical damage, dehydration, and bacteria infiltration, as well as coordinate the gaseous exchange. On the other side, the SF_HA layer acts as a wound-dressing interface able to absorb wound exudate, promote nutrient exchange, support cell adhesion and proliferation as well as confer antimicrobial, anti-inflammatory and antioxidant properties to the membrane due to the incorporation of THY (SF_HA_THY).

The morphology of the nanofibers were analyzed by SEM and the diameters of the fibers were determined using the Image J software (Fig. 1). The size measurements revealed that the nanofibers of the top layer display an average diameter of 471.4 ± 151.6 nm, while the SF_HA and SF_HA_THY nanofibers of the bottom layer present a mean diameter of 270.0 ± 82.2 nm and 295.4 ± 88.4 nm, respectively. Moreover, to improve the water stability of the SF a crosslinking process was performed, resulting in an increase in the SF_PCL, SF_HA, and SF_HA_THY nanofibers mean diameter to 615.9 ± 190.4 nm, 306.8 ± 85.6 nm and 412.7 ± 106.7 nm, respectively. Cross-sectional images of the EAM were also acquired (Fig. 2) and they clearly show the bilayered organization of the produced membrane. Furthermore, the incorporation of THY did not induce any significant morphologic variations in the bottom layer of the membrane, *i.e.* size and structure. Contrarily, the crosslinking process leads to the formation of more irregular nanofibrous structures with increased density and fiber diameters, which is in agreement with the data available in the literature for similar crosslinked nanofibrous meshes [14,15]. Nevertheless, the nanofibers diameter is still within the range of the collagen fibrils found at the ECM (50–500 nm), which highlights the EAM capacity to mimic some of the native skin structural features and provide an interface that favours cell migration, adhesion, and proliferation [16].

### 3.2. Attenuated total reflectance-Fourier transform infrared spectroscopic analysis

As aforementioned, the aqueous stability of SF can be improved by promoting a conformational change in its structure, *i.e.* a conversion from random coil to β-sheet through the treatment of the membrane with ethanol vapor. The structural changes in SF were confirmed by FTIR analysis. In Fig. S3, it is possible to see that the peaks of amide I (1643 $cm^{-1}$) and amide II (1528 $cm^{-1}$) that are characteristic of the random coil conformation were shifted to 1627 $cm^{-1}$ and 1518 $cm^{-1}$, respectively. This result confirms the presence of the β-sheet conformation of SF nanofibers and consequently the improved aqueous stability of SF [15,17]. Further, to confirm the improved water stability, the membranes were also incubated for 24 h in ultrapure water and the absorbance at 275 nm was recorded. The spectrum of the crosslinked membranes did not show a significant release of SF, while the spectrum of uncrosslinked membranes presents a broad peak, *i.e.* SF dissolution occurred.

On the other side, FTIR was also used to characterize the chemical composition of the electrospun layers produced in this work (Fig. 3A). The spectrum of the top layer displays the characteristic peaks of SF at 3281 $cm^{-1}$ (–OH stretching and bending vibration mode), 2942 $cm^{-1}$ (asymmetric $CH_2$ stretching), 1627 $cm^{-1}$ (amide I), and 1518 $cm^{-1}$ (amide II) [15,18]. Additionally, in this spectrum, the characteristic peaks of PCL are also visible at 2942 $cm^{-1}$ (asymmetric $CH_2$ stretching), 1724 $cm^{-1}$ (carbonyl stretching), 1293 $cm^{-1}$ (C—O and C—C stretching), 1239 $cm^{-1}$ (asymmetric C—O—C stretching) and 1163 $cm^{-1}$ (symmetric C—O—C stretching) [18]. Similarly, the spectrum of the bottom layer (Fig. 3B) shows the typical bands of SF, as well as the characteristic peaks of HA at 3200–3600 $cm^{-1}$ (OH and NH stretching), 1640–1690 $cm^{-1}$ (C═O stretching of primary amide) and 1029 $cm^{-1}$ (C—O—C stretching) [5].

Furthermore, the incorporation of THY into SF_HA nanofibers was also investigated. The spectrum presented in Fig. S5 displays the THY characteristic peaks at 3174 $cm^{-1}$ (stretching vibration of phenolic O—H group), 2900 $cm^{-1}$ region (C—H stretching), 1619–1516 $cm^{-1}$ (C—C ring stretching band), 1516–1421 $cm^{-1}$ (OH bending vibration), 1243 $cm^{-1}$ (C—O stretching), and 801 $cm^{-1}$ (aromatic C—H bending) [19]. Further, the same peaks can be observed in the spectrum of the SF_HA_THY membrane, which indicates the successful entrapment of THY within the polymeric nanofibers.

### 3.3. Characterization of the membranes' mechanical properties

The mechanical properties of the produced EAM were assessed in dry and wet conditions. The Young's modulus, tensile strength, and

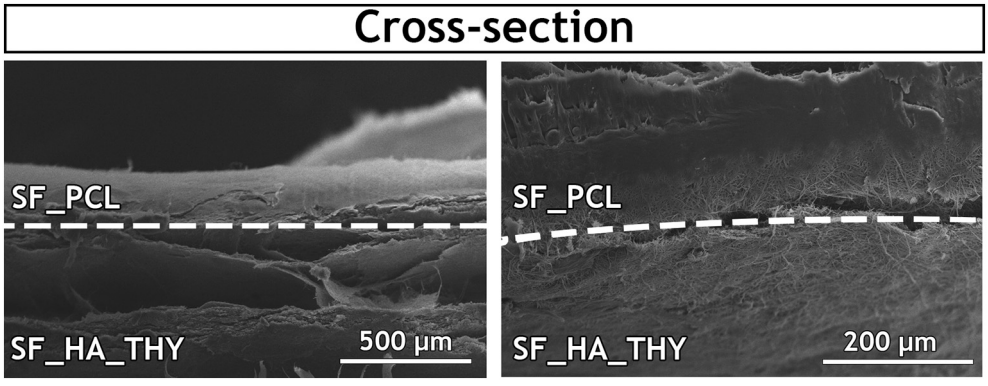


**Fig. 2.** SEM images of the produced EAM cross-section (top layer: SF_PCL; bottom layer: SF_HA).

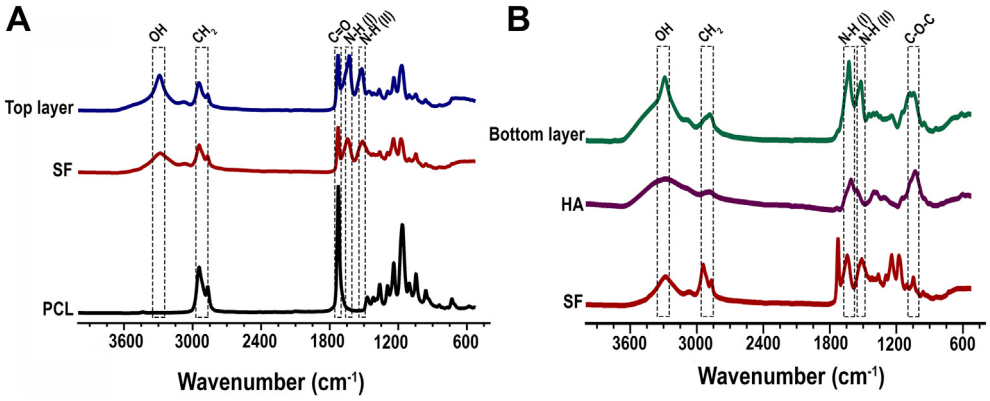


**Fig. 3.** ATR_FTIR analysis of the top (A) and bottom (B) nanofibrous layers as well as of its raw materials.

elongation at break for the EAM and the values reported for native skin are presented in Table S1. The Young's modulus obtained for EAM was 25.67 ± 6.84 MPa in a dry state, whereas in wet conditions this value decreased to 14.70 ± 4.42 MPa. Moreover, the EAM showed values of the Tensile Strength of 23.01 ± 6.73 MPa in the dry state and 7.59 ± 1.26 MPa in wet conditions. The elongation at break assays reveal that the EAM can bear a strain of 69.27 ± 14.87% and 57.39 ± 13.78% for the dry and wet state, respectively. The obtained data, both in dry and wet conditions, emphasize the excellent mechanical properties of the EAM. In fact, the obtained Young modulus, tensile strengths, and elongation-at-break values are similar to those displayed by the native skin (as depicted in Table S1). Further, such results demonstrate that the EAM can tolerate all the stresses during the membrane handling and provide mechanical support during the wound healing process. The mechanical performance of EAM can be attributed to PCL and SF, which are recognized by their good mechanical properties [6,20–22]. Further, Nogueira et al. reported that the structural transition from random coil to β-sheet conformation makes SF more resistant to water and also improves its mechanical properties [23].

### 3.4. Assessment of the membranes' porosity

The wound dressings' porosity affects the cellular adhesion, infiltration, and proliferation, as well as gases, nutrients and fluids exchange at the wound site [24]. Based on data available in the literature, for an effective healing process occurs, wound dressings should display porosity values within the range of 60–90% [25].

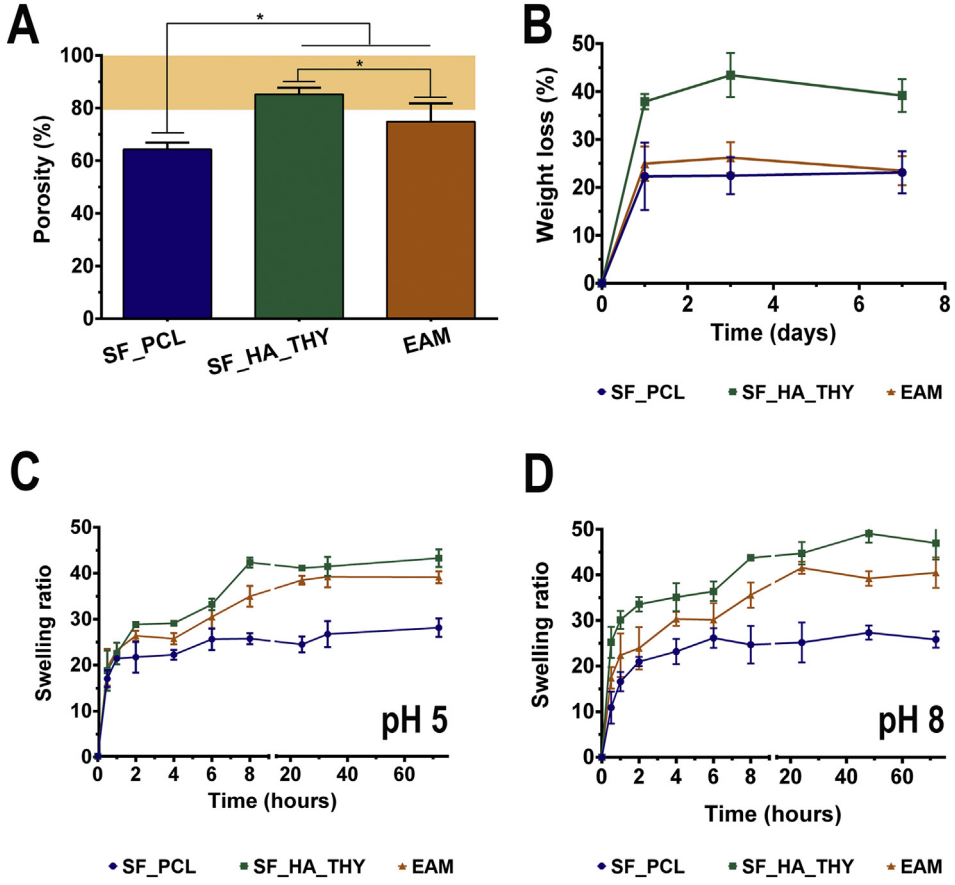


**Fig. 4.** Characterization of the total porosity (A), weight loss (B), and swelling profile at pH 5 (C) and pH 8 (D), of the SF_PCL and SF_HA_THY layers and EAM at different time points (data are presented as the mean ± standard deviation, n = 5, *p < 0.05).

Herein, the SF_PCL and SF_HA_THY nanofibrous layers presented a total porosity of 64.28 ± 2.59% and 85.24 ± 2.47%, respectively (Fig. 4A). Moreover, the EAM membrane displayed a total porosity of 74.78 ± 6.98%, a value that is comprehended between the porosity values of the individual membranes (top and bottom layers). The obtained porosity values are in accordance with the structural differences noticed between the top and bottom layers, as previously observed in the SEM images. In fact, the lower porosity of SF_PCL layer is justified by the increased nanofiber diameter and deposition density. Such values are in agreement with those obtained for other asymmetric membranes reported in the literature, where the top layer produced with PCL displayed the lowest porosity (55 ± 5%) and the bottom layer composed of CS_AV_PEO showed a superior porosity (97.8 ± 5%) [6]. Moreover, the obtained porosity values are compatible with the functions desired for each layer, the lower porosity of top layer will inhibit microorganism invasion whereas the highly porous bottom layer (~90%) allows cell adhesion, migration, and proliferation [24].

### 3.5. Evaluation of the swelling profile of the produced membranes

Membranes' swelling capacity has a tremendous impact on its application in the wound healing process. This property is fundamental to accomplish the absorption of the wound exudate, which is essential to prevent tissue maceration and skin infection [26]. The swelling profile of the produced membranes was studied by incubating them in PBS at pH = 5 (Fig. 4C) and pH = 8 (Fig. 4D) to mimic the conditions found in the native and injured skin. The obtained results demonstrated that SF_PCL, SF_HA _THY, and EAM membranes reached their maximum water uptake capacity after 24 h. On the other hand, the swelling capacity for all the groups was higher at pH 8, *i.e.* water absorption ratio of ≈25, ≈45 and ≈42 for SF_PCL, SF_HA_THY, and EAM, respectively. The obtained data reveal that the bottom layer presents a higher swelling ratio in comparison with the top layer, which occurs due to the incorporation of hydrophilic compounds, like HA [27]. Further, the combination of SF_PCL and SF_HA_THY nanofibrous layers appears to result in an EAM membrane with a more controlled swelling capacity, *i.e.* have a higher swelling ratio than the top layer, however it is not as high as the bottom layer, which allows a sustained absorption of exudates and avoids the wound dehydration. Additionally, the increased swelling capacity at pH 8 highlights the potential of EAM to remove the exudate from the wound, produced 1–3 days after the injury occurs, namely during the inflammatory phase.

### 3.6. Evaluation of the membranes' degradation profile

When a non-biodegradable biomaterial is used to cover the skin lesion, its removal from the wound can induce the formation of scar tissue and pain to the patient as well as increase the risk of bacterial contamination. In this way, wound dressings should be produced with biodegradable materials, that display a degradation profile that is similar to the skin regeneration rate [28]. Therefore, the fine-tuning of the biomaterials degradation profile is crucial to enhance the healing process [29].

SF fibers are defined as a non-degradable biomaterial, which hinders its application in the production of wound dressings. To surpass such handicap, in this study, silk-based EAM degradability was tailored by adding different polymers and compounds to the SF matrix (Fig. 4C). The degradation studies showed that the EAM membrane undergoes a weight loss of 23% during the 7 days. Further, SEM images of the EAM membrane cross-section (Fig. S6) were acquired and revealed that the two layers remain attached together, even after incubation in PBS for 7 days. The degradation profile may be justified by the strong entanglement between the two layers that compose the EAM. Moreover, the two polymers used in the top layer (SF and PCL) present a slow degradation profile. In fact, the *in vitro* degradation of SF occurs mainly by hydrolysis, whereas PCL degrades through the action of metalloproteinases and hydrolysis of the polyester components [21]. In turn, the HA and THY, present in the bottom layer of EAM, are characterized by suffering higher weight losses *in vivo*. HA is degraded by the action of the hyaluronidases enzymes, hydrolysis and oxidation [9]. On the other hand, THY suffers degradation through the oxidation, polymerization, disproportionation and cyclization reactions [30].

### 3.7. Characterization of the EAM water vapor transmission rate

The ability of a wound dressing control the water loss can be determined by the Water Vapor Transmission Rate (WVTR) [31]. In the wound healing process, WVTR plays an important role in preventing wound dehydration and exudate accumulation, favouring the tissue regeneration [32].

The EAM membrane presented a WVTR of 2070.62 ± 102.52 mL/-$m^2$/day. This value is superior to those found on commercial wound dressings (*e.g.* 491 ± 44 g/$m^2$/day for Tegaderm™ (3 M), 394 ± 12 g/$m^2$/day for Bioclusive™ (Johnson-Johnson), and 792 ± 32 g/$m^2$/day for Opsite (Smith & Nephew)) [33] and to other asymmetric membranes previously described in the literature (*e.g.* asymmetric PCL/CS_AV_PEO membrane (1252.35 ± 21.22 g/$m^2$/day) [6], PCL_HA/CS_Zein electrospun bilayer membrane (1762.91 ± 187.50 g/$m^2$/day) [5] and asymmetric PVA/CS membranes produced by $scCO_2$-assisted phase inversion method (214 ± 16 g/$m^2$/day) [34]). In fact, according to the data available in several studies, the ideal WVTR value should be comprised between 2000 and 2500 mL/$m^2$/day to facilitate the proliferation and function of epidermal cells and fibroblasts as well as the water vapor exchanges [35].

### 3.8. Water contact angle determination

Wound dressing material wettability is one of the most important surface properties that affect its biological performance, namely protein adsorption, platelet adhesion, blood coagulation as well as cells and bacterial adhesion [36]. Herein, materials wettability was studied by determining the water contact angle (WCA). The SF_PCL layer exhibited a WCA value of 103.10 ± 6.57°, revealing a hydrophobic character. This result can be explained by the hydrophobicity of the PCL aliphatic polyester chains and SF β-sheet conformation [15,17]. Further, the SF_PCL membrane was designed to act as a physical barrier that protects the wound and also avoids bacteria infiltration. For that purpose, the application of hydrophobic surfaces (90° < WCA < 150°) has been reported as more effective [5,36]. In turn, the SF_HA and SF_HA_THY layers presented WCA values of 26.51 ± 4.87° and 38.77 ± 5.32°, respectively. This hydrophilic character is explained by the presence of HA polymer, which is one of the most hydrophilic molecules of ECM [53]. Furthermore, the incorporation of hydrophobic essential oil (THY) resulted in a membrane with a moderate hydrophilic surface, WCA values comprehended between 40°–70°, which are considered ideal for supporting cell attachment and proliferation (see Section 3.11) [37]. Such differences in wettability between the top and bottom layers were also verified in other asymmetric membranes described in the literature [5,6].

### 3.9. Characterization of the thymol in vitro release profile

Different materials and drugs have been used to produce electrospun meshes, that are aimed to be used as drug delivery systems [5,38]. Among them, biodegradable (*e.g.* CS, poly(lactic acid), poly(ethylene oxide), PCL [5,39]) or non-biodegradable (*e.g.* polyurethane [40]) materials have been used to accomplish specific drug release profiles. Herein, THY (an herbal drug) was selected to be loaded into the nanofibers in order to provide antibacterial and antioxidant properties to the bottom layer of the EAM. The LE and EE values obtained for the THY incorporation in the bottom layer of the EAM were 64.8 ± 5.42% and 79.7 ± 7.19%, respectively. These results indicated that THY can

be efficiently encapsulated in the SF_HA nanofibrous layer by using the electrospinning technique.

Afterwards, the THY release profile from SF_HA nanofibrous layer was characterized at pH 5 (pH of the native skin) and 8 (pH of injured skin) [7]. The obtained results (Fig. 5B) show that the THY release from the nanofibers, at both pHs, comprises two different phases, *i.e.* a burst release in the first 8 h after immersion in PBS, followed by a gradual release up to 24 h. Such release profile can be justified by the high surface to volume ratio of the nanofibers that favours the PBS adsorption and consequently the diffusion of THY from the nanofibrous membranes to the release media. The cumulative release of THY from the bottom layers is 71.75 ± 2.06% and 91.87 ± 0.99% at pH 5 and pH 8, respectively. Such results may be explained by the higher swelling exhibited by the membranes at pH 8. Further, the increased HA degradation that occurs in alkaline conditions can favour the release of THY [42]. Nevertheless, the obtained release profile is crucial for the bottom layer to avoid the skin infections as well as to reduce the formation of reactive oxygen species at wound site.

Moreover, the release data was also analyzed by different mathematical kinetic models to characterize the type of interactions that affect the drug release, please see Table S2. The mathematical model that presents the best fitting with the obtained release data is the Korsmeyer-Peppas ($R^2 = 0.99$ ($n < 0.5$)). This indicates that the drug is released from the SF_HA_THY layer through a Fickian diffusion process, which occurs through the swelling of the polymeric matrix and the formation of heterogeneous regions with a quicker drug dissolution in the composite nanofiber [41]. Additionally, due to the higher weight loss of the bottom layer (as previously determined), the release mechanism could also be fitted with the Hixon-Crowell model ($R^2 = 0.92$). Therefore, it can be concluded that the drug release from SF_HA_THY layer occurs essentially due to the THY dissolution from the polymeric matrix and the degradation of the nanofibers.

### 3.10. Evaluation of the antioxidant activity of the produced membranes

During the wound healing process, namely in the inflammatory phase, occurs the production of reactive oxygen species (ROS), which are important molecules in the body defence against the microorganisms' invasion. However, when the production of ROS is excessive, the ECM proteins are degraded, and cell functions are impaired. Moreover, the ROS can prompt the proinflammatory cytokines secretion and promote the activity of matrix metalloproteases, impairing the production of ECM and, consequently, delaying the healing process [43].

Herein, the antioxidant activity of the produced membranes was investigated through the DPPH assay, along 8 h. DPPH is a stable free radical, which displays a maximum absorption peak at 517 nm. In Fig. 5C, it is observed that SF_PCL and SF_HA membranes present a reduced antioxidant activity (9.22% and 14.15%, respectively). On the other hand, SF_HA_THY membrane exhibited high DPPH scavenging activity (≈45.64%) after 8 h of incubation. The residual antioxidant activity of SF_PCL and SF_HA is attributed to the phenolic side chains of SF tyrosine and tryptophan amino acids residues [15]. In the bottom layer, the THY incorporation in the SF_HA nanofibers improved its antioxidant activity. In the literature, Yanishlieva and their collaborators already highlighted the antioxidant activity of THY in a lipidic mixture (*i.e.* purified triacylglycerols of lard and sunflower oil) [12]. This protective effect of THY arises from its capacity to donate a hydrogen atom (from the phenol hydroxyl groups) to the peroxyl radicals, producing stabilized phenoxyl radicals [44].

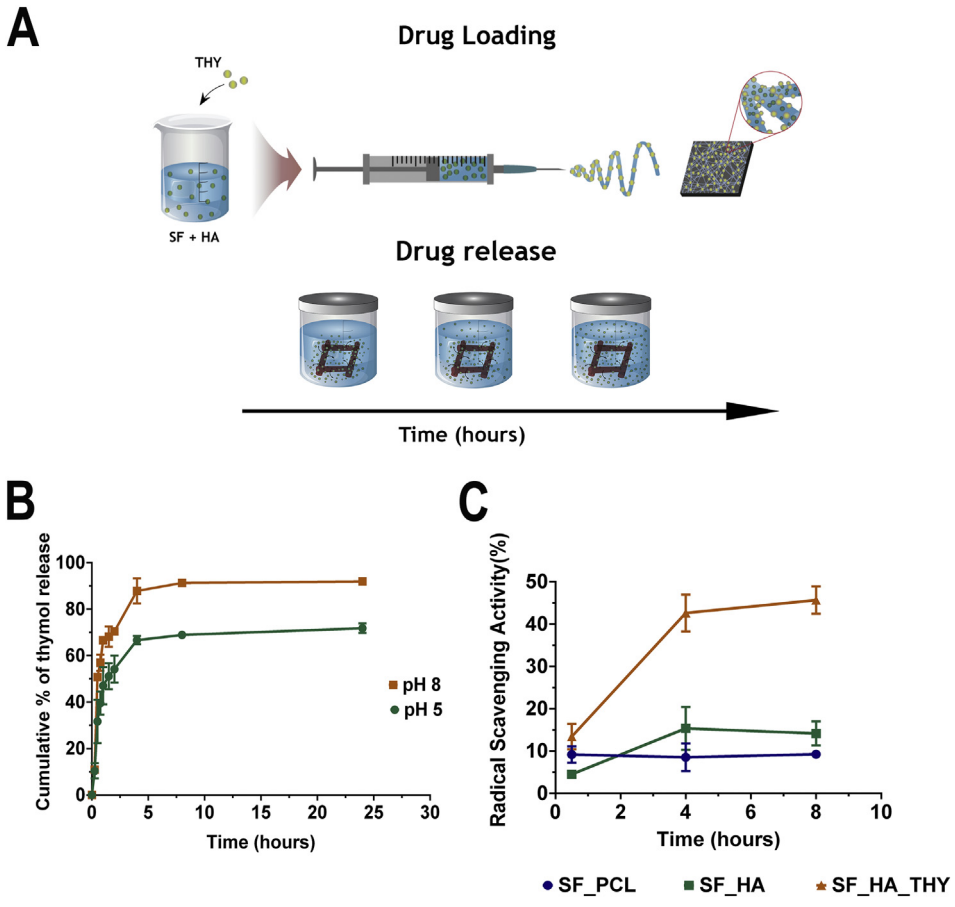


**Fig. 5.** Schematic representation of the drug loading and release assays (A); evaluation of the THY *in vitro* release profile (B) and antioxidant activity (C).

### 3.11. Characterization of the biological properties of the electrospun membranes

#### 3.11.1. Evaluation of the cell viability and adhesion in contact with the EAM

The cytocompatibility of the electrospun membranes was evaluated using NHDF as model cells. Fibroblasts were chosen since they are involved in the production of ECM, glycoproteins, adhesive molecules, and various cytokines that modulate the reestablishment of the damaged tissue.

The optical microscopic images of the NHDF cells seeded in contact with membranes after 1, 3 and 7 days (Fig. S7) show that cells did not suffer any morphological alteration since they exhibit a morphology similar to those present in the negative control (cells incubated only with culture medium). On the other side, cells with a spherical shape were visualized in the positive control. Furthermore, the cytotoxic profile of the membranes was also evaluated through a MTS assay, over 1, 3 and 7 days (Fig. 6A). The data obtained show that the produced membranes did not induce any cytotoxic effect on NHDFs, over 7 days. Moreover, the amount of THY incorporated in the membranes did not compromise the cell viability.

In addition, the membranes biocompatibility was also characterized by the dsDNA assay. The obtained results (Fig. 6B) do not show any significative differences between the test and the control group, which suggests that the NHDFs remain viable and proliferate when seeded in contact with the produced membranes for 7 days.

Moreover, the SEM images presented in Fig. 6C show that the topography and roughness of the electrospun membranes promote cell adhesion. However, in the SF_HA and SF_HA_THY layers, the fibroblast cells appear to present more filopodia protrusions, showing higher cell adhesion and proliferation.

#### 3.11.2. Live/dead assay

Live/dead assay was also performed to analyse the cell survival at the surface of the membranes, by simultaneously staining live (green labelled) and dead (red labelled) cells. The CLSM images (Fig. 7) clearly show that cells remain viable when they are seeded in contact with membranes, and their number increased along time. These results corroborate the data obtained in the MTS and dsDNA assays, thus supporting the biocompatibility of these membranes. Moreover, the SF_HA and SF_HA_THY layers present a higher number of cells. The enhanced biological properties exhibited by the bottom layers are explained by the presence of HA in its composition. In fact, HA is a protein found in skin ECM that has a high water retention capacity, stimulates the migration of inflammatory and fibroblast cells into the wounds, through its interaction with cell surface receptors CD44 [45]. Moreover, the low molecular weight of the HA used in this study also favours cell migration and adhesion [46]. Indeed, these superior biological performance of HA enriched nanofibers was also observed in a study performed by Li et al., where the incorporation of HA improved the cellular microenvironment, favouring the cellular infiltration and adhesion to the nanofibers [47]. Moreover, Selvaraj and their co-workers also demonstrated that fibroblasts proliferate and remain viable when in contact with SF electrospun membranes [15]. Overall, the obtained results clearly demonstrate the excellent biocompatibility of the produced EAM as well as support its application as a wound dressing for promoting the healing process.

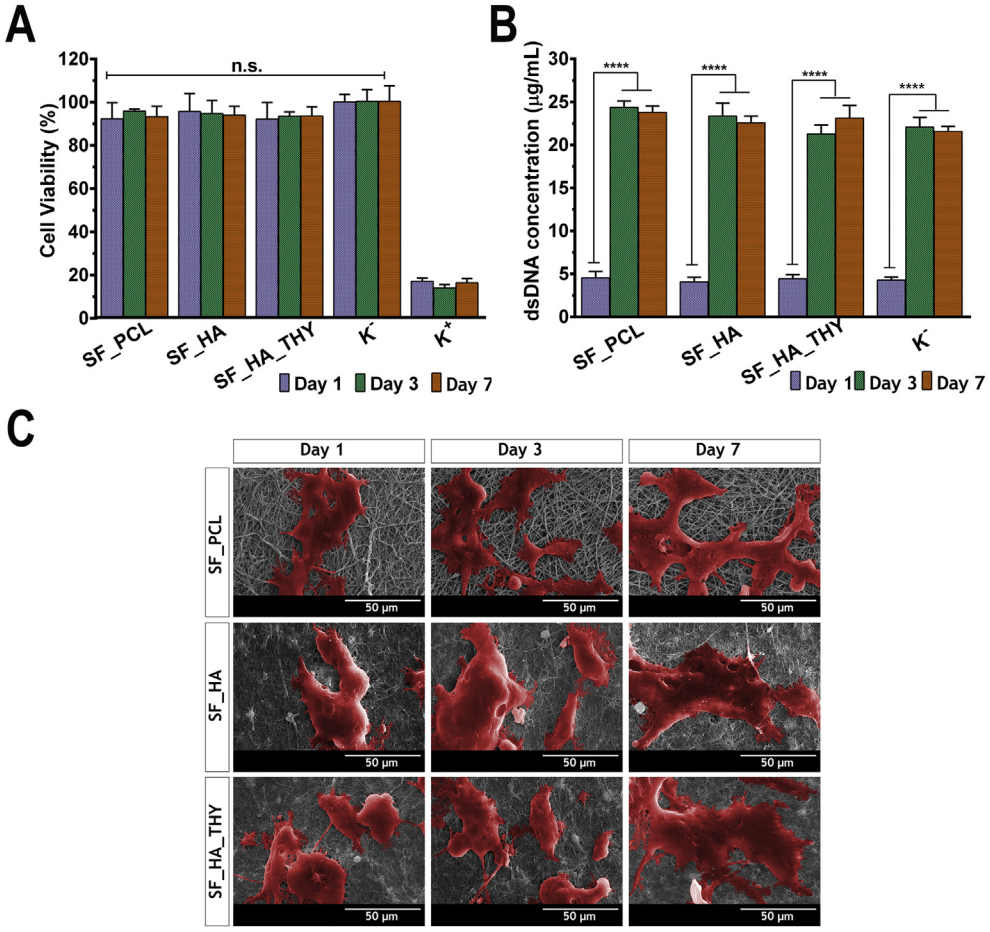


**Fig. 6.** Characterization of the produced membranes cytotoxic profile. Analysis of the NHDF cell viability (A) and dsDNA content (B) after 1, 3, and 7 days of incubation with the membranes. Data are presented as the mean ± standard deviation, n = 5, ****p < 0.0001. SEM images of NHDF cells seeded at the surface of the different electrospun membranes after 1, 3, and 7 days (C).

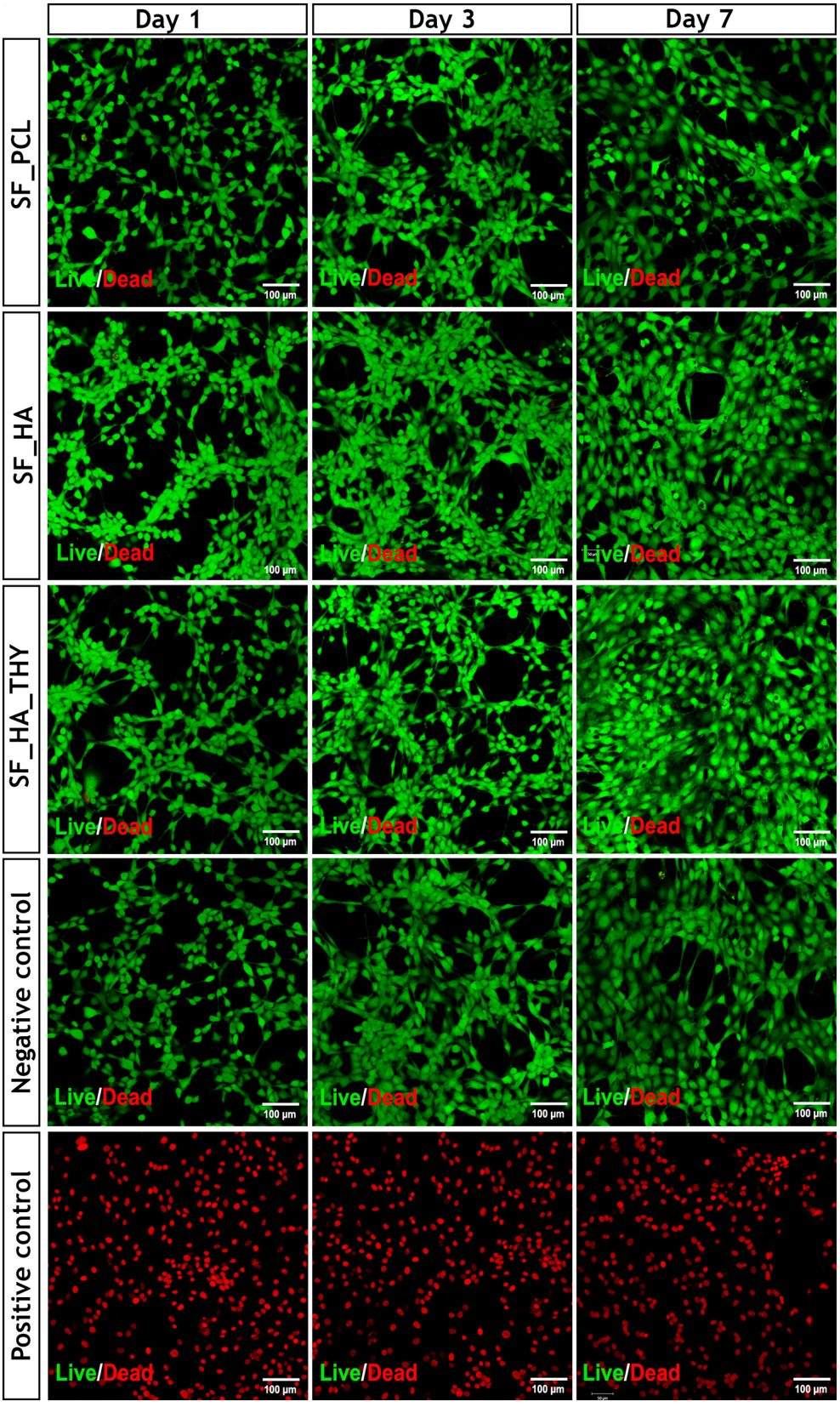


**Fig. 7.** Fluorescence microscopic images from a Live-dead assay of NHDFs cultured on the surface of the produced membranes after, 1, 3 and 7 days. Green channel: viable cells labelled with Calcein; red channel: dead cells stained with Propidium iodine.

### 3.12. Evaluation of the antimicrobial properties of the membranes

Bacterial contaminations, which usually occur after a skin injury, are regarded as one of the most severe and devastating health complications. According to the available information, up to 65–80% of all infections lead to the formation of biofilms, highlighting the urgent need to develop biomaterials capable of avoiding the establishment and development of infections [48]. In this context, the antimicrobial properties of the produced membranes were evaluated by using *S. aureus* (gram-positive bacterium) and *P. aeruginosa* (gram-negative bacterium) as bacteria models. These strains were selected since they are described as the most common microorganisms found in skin infections [49].

The results presented in Fig. 8A and B show that the top layer (SF_PCL) of the EAM membrane, acts as a protective barrier, avoiding the bacterial infiltration in both bacterial models. Further, the obtained results do not show any significant difference with the control group, a filter paper (pore size of 0.22 μm). Additionally, SEM images (Fig. 8C) also demonstrate that the bacteria can adhere to the upper side of the top layer, however no bacteria were visualized at the bottom side of the nanofibrous layer, which emphasizes the capacity of the top layer to act as a filter, due to its low porosity, avoiding the microorganism's colonization of the wound.

Furthermore, the antibacterial properties of the bottom layers (SF_HA and SF_HA_THY) were also evaluated. To accomplish that, bacteria models (*S. aureus* and *P. aeruginosa*) were grown in contact with the membranes and then, the number of bacterial colonies formed was counted. The obtained results show that the SF_HA_THY membranes present an increased inhibitory effect in bacterial growth, 87.42% and 58.43% for *S. aureus* and *P. aeruginosa*, when compared to SF_HA membranes, 4.05% and 3.42% for *S. aureus* and *P. aeruginosa* (Fig. 9A and B). Furthermore, contrasting to SF_HA membranes, no biofilm formation was observed at the surface of SF_HA_THY nanofibrous layer (Fig. 9C). To further assess the antibacterial potential of the membranes, the modified Kirby-Bauer assay was performed. The obtained data confirmed the excellent antimicrobial properties of the SF_HA_THY layer, which presented a 2 to 3 times larger inhibitory halo area in comparison to SF_HA layer for *S. aureus* and *P. aeruginosa*, respectively (Fig. S8).

The results demonstrate that the incorporation of THY conferred antimicrobial properties to the bottom SF_HA layer. The antibacterial properties of essential oils and their components have been already reported in the literature [50,51]. In the majority of the cases, the essential oils destabilize the cellular architecture, leading to the disruption of the cell wall structure and functions [52,53]. The impairment of the cell wall permeability can compromise the solutes transport, the maintenance of the cell energy, and the metabolic regulation [54]. Further, the antibacterial activity of essential oils can induce the reduction of the membrane potential, the disruption of the proton pumps, and depletion of the intracellular ATP [55]. However, several studies speculate that the antimicrobial activity of essential oils is significantly influenced by the physicochemical characteristics of the bacterial cell wall [52,56]. Indeed, in this study, the THY presented a superior efficacy towards *S. aureus*. In this sense, some studies suggest that the difference in the susceptibility to antimicrobials between Gram-positive and Gram-negative bacteria could be attributed to the cytoplasmic membrane and/or outer membrane cell wall structure and composition [57]. The structure of the Gram-positive bacteria cell wall facilitates the penetration of hydrophobic molecules into the cells, allowing their action on the cell wall and

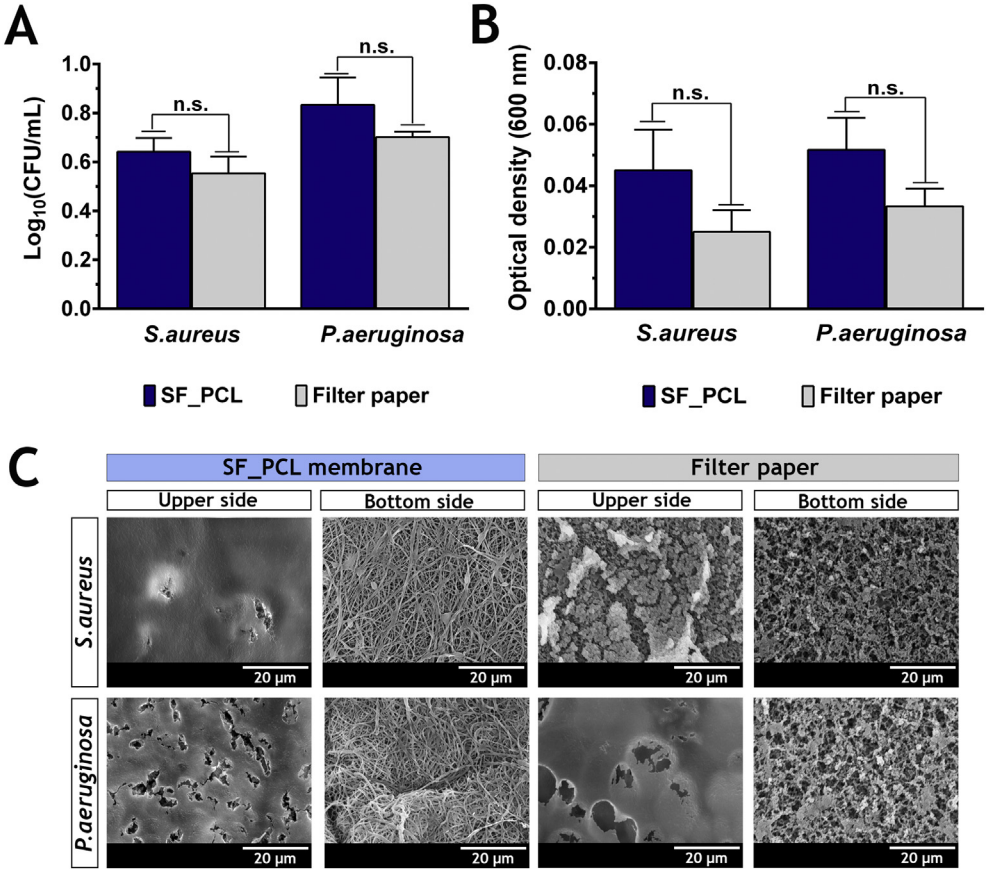


**Fig. 8.** Evaluation of the bacterial infiltration through SF_PCL membrane and filter paper (control group). Determination of the number of the CFU of *S. aureus* and *P. aeruginosa* that crossed the SF_PCL membrane or filter paper, after 24 h (A). Measurement of the optical density from medium samples recovered from the lower chamber of the transwell system (B). Data are presented as the mean ± standard deviation, n = 5, n.s. = non-significant. SEM images of the microorganisms (*S. aureus* and *P. aeruginosa*) that adhered to the upper or lower side of the SF_PCL membrane and filter paper (C).

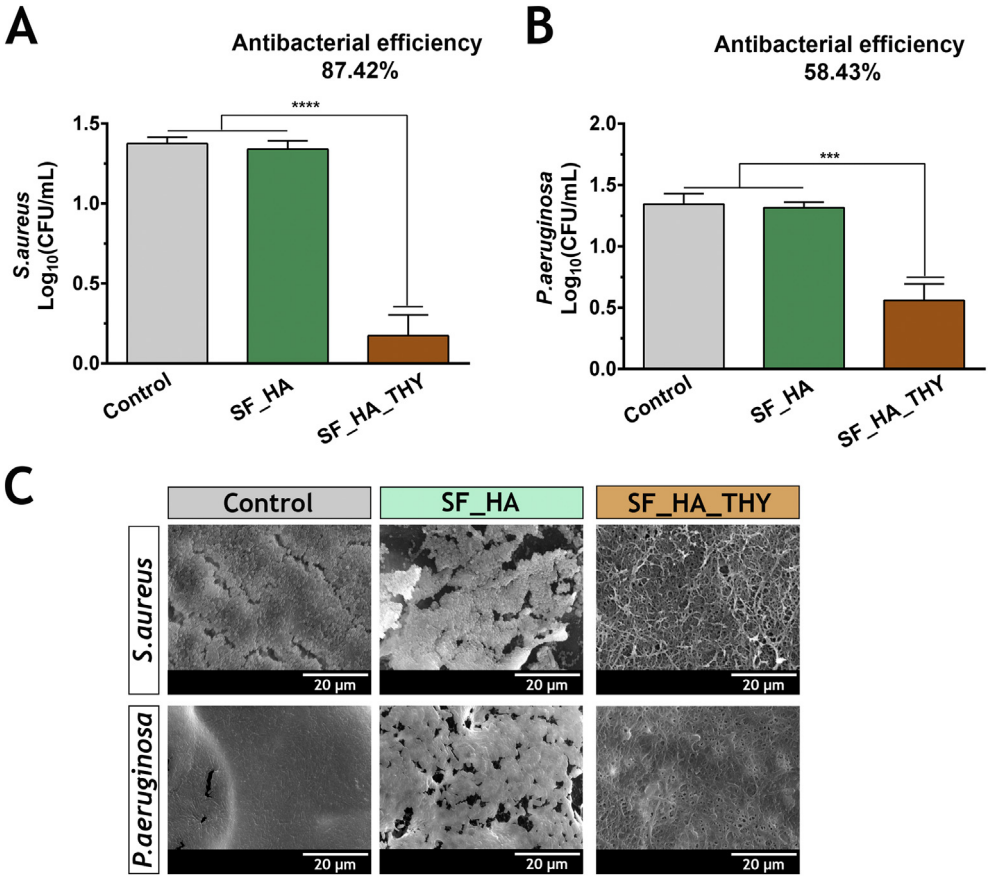


**Fig. 9.** Evaluation of the antibacterial potential of the SF_HA and SF_HA_THY nanofibrous layers against *S. aureus* (A) and *P. aeruginosa* (B). Data are presented as the mean ± standard deviation, n = 5, ***p < 0.001, ****p < 0.0001. SEM images of control, SF_HA and SF_HA_THY nanofibrous layers incubated with *S. aureus* and *P. aeruginosa* (C).

within the cytoplasm [57]. On the other hand, the cell wall of Gram-negative bacteria is more complex and presents a higher thickness [56]. Further, the cell wall of the Gram-negative bacteria is composed primarily of lipopolysaccharide molecules which form a hydrophilic permeable barrier, providing protection against the effect of hydrophobic essential oils [58].

## 4. Conclusion

Despite the tremendous efforts made in the development of wound dressings, none of the currently available is fully capable of re-establish the skin native structure and functions. To overcome this situation, the electrospun asymmetric membranes exhibiting a skin-like layered organization and physicochemical properties arise as a highly promising approach for improving the wound healing mechanism. Herein, a bilayered EAM was produced using as the main component a silk derived biopolymer. The top layer was manufactured with SF and PCL to act as a physical barrier at the wound site, whereas the bottom layer was composed of SF, HA and THY to enhance the wound healing process and avoid the occurrence of infections at the wound site. It is worth to notice that to the best of our knowledge, this is the first time that THY is incorporated in an EAM. Moreover, the structural organization and mechanical properties exhibited by EAM are similar to those of the human native skin. Moreover, *in vitro* assays revealed that the membrane can promote the cell adhesion, proliferation and spreading. In addition, the incorporation of THY into the bottom nanofibrous layer imprinted in the EAM antioxidant and antibacterial properties that are essential for the healing process.

In the near future, the EAM and THY anti-inflammatory, local anesthetic, antinociceptive, cicatrizing and antiseptic properties will be further characterized to reinforce the application of this membrane as a wound dressing. Moreover, the inclusion of growth factors and proteins can also be considered to improve the biological performance of these membranes.

## Acknowledgments

The authors would like to acknowledge Abílio Silva for the help in the mechanical assays. Financial support was provided by FEDER funds through the POCI—COMPETE 2020—Operational Programme Competitiveness and Internationalization in Axis I—Strengthening research, technological development and innovation (Project POCI-01-0145-FEDER-007491) and National Funds by FCT—Foundation for Science and Technology (Project UID/Multi/00709/2013). Sónia P. Miguel and André F. Moreira acknowledges their Ph.D. fellowships from FCT (SFRH/BD/109563/2015 and SFRH/BD/109482/2015, respectively).

## Appendix A. Supplementary data

Supplementary data to this article can be found online at https://doi.org/10.1016/j.ijbiomac.2018.10.041.

## References

[1] A.A. Chaudhari, K. Vig, D.R. Baganizi, R. Sahu, S. Dixit, V. Dennis, S.R. Singh, S.R. Pillai, Future prospects for scaffolding methods and biomaterials in skin tissue engineering: a review, Int. J. Mol. Sci. 17 (12) (2016) 1974.
[2] B.K. Sun, Z. Siprashvili, P.A. Khavari, Advances in skin grafting and treatment of cutaneous wounds, Science 346 (6212) (2014) 941–945.
[3] R.F. Pereira, C.C. Barrias, P.L. Granja, P.J. Bartolo, Advanced biofabrication strategies for skin regeneration and repair, Nanomedicine 8 (4) (2013) 603–621.
[4] S.P. Miguel, D.R. Figueira, D. Simões, M.P. Ribeiro, P. Coutinho, P. Ferreira, I.J. Correia, Electrospun polymeric nanofibres as wound dressings: a review, Colloids Surf. B: Biointerfaces 169 (2018) 60–71.

[5] D.R. Figueira, S.P. Miguel, K.D. de Sá, I.J. Correia, Production and characterization of polycaprolactone-hyaluronic acid/chitosan-zein electrospun bilayer nanofibrous membrane for tissue regeneration, Int. J. Biol. Macromol. 93 (2016) 1100–1110.
[6] S.P. Miguel, M.P. Ribeiro, P. Coutinho, I.J. Correia, Electrospun polycaprolactone/aloe vera_chitosan nanofibrous asymmetric membranes aimed for wound healing applications, Polymer 9 (5) (2017) 183.
[7] P.I. Morgado, S.P. Miguel, I.J. Correia, A. Aguiar-Ricardo, Ibuprofen loaded PVA/chitosan membranes: a highly efficient strategy towards an improved skin wound healing, Carbohydr. Polym. 159 (2017) 136–145.
[8] H. Wang, X.Y. Liu, Y.J. Chuah, J.C. Goh, J.L. Li, H. Xu, Design and engineering of silk fibroin scaffolds with biomimetic hierarchical structures, Chem. Commun. 49 (14) (2013) 1431–1433.
[9] M.N. Collins, C. Birkinshaw, Hyaluronic acid based scaffolds for tissue engineering—a review, Carbohydr. Polym. 92 (2) (2013) 1262–1279.
[10] Z. Karami, I. Rezaeian, P. Zahedi, M. Abdollahi, Preparation and performance evaluations of electrospun poly (ε-caprolactone), poly (lactic acid), and their hybrid (50/50) nanofibrous mats containing thymol as an herbal drug for effective wound healing, J. Appl. Polym. Sci. 129 (2) (2013) 756–766.
[11] M. Marino, C. Bersani, G. Comi, Antimicrobial activity of the essential oils of *Thymus vulgaris* L. measured using a bioimpedometric method, J. Food Prot. 62 (9) (1999) 1017–1023.
[12] N.V. Yanishlieva, E.M. Marinova, M.H. Gordon, V.G. Raneva, Antioxidant activity and mechanism of action of thymol and carvacrol in two lipid systems, Food Chem. 64 (1) (1999) 59–66.
[13] L. Fan, H. Wang, K. Zhang, C. He, Z. Cai, X. Mo, Regenerated silk fibroin nanofibrous matrices treated with 75% ethanol vapor for tissue-engineering applications, J. Biomater. Sci. Polym. Ed. 23 (1–4) (2012) 497–508.
[14] P. Ferreira, P. Santos, P. Alves, M.P. Carvalho, K.D. de Sá, S.P. Miguel, I.J. Correia, P. Coimbra, Photocrosslinkable electrospun fiber meshes for tissue engineering applications, Eur. Polym. J. 97 (2017) 210–219.
[15] S. Selvaraj, N.N. Fathima, Fenugreek incorporated silk fibroin nanofibers a potential antioxidant scaffold for enhanced wound healing, ACS Appl. Mater. Interfaces 9 (7) (2017) 5916–5926.
[16] J. Zhao, W. Han, H. Chen, M. Tu, R. Zeng, Y. Shi, Z. Cha, C. Zhou, Preparation, structure and crystallinity of chitosan nano-fibers by a solid–liquid phase separation technique, Carbohydr. Polym. 83 (4) (2011) 1541–1546.
[17] J. Kong, S. Yu, Fourier transform infrared spectroscopic analysis of protein secondary structures, Acta Biochim. Biophys. Sin. 39 (8) (2007) 549–559.
[18] L. Ghasemi-Mobarakeh, M.P. Prabhakaran, M. Morshed, M.-H. Nasr-Esfahani, S. Ramakrishna, Electrospun poly (ε-caprolactone)/gelatin nanofibrous scaffolds for nerve tissue engineering, Biomaterials 29 (34) (2008) 4532–4539.
[19] M. Michalska-Sionkowska, M. Walczak, A. Sionkowska, Antimicrobial activity of collagen material with thymol addition for potential application as wound dressing, Polym. Test. 63 (2017) 360–366.
[20] M. Labet, W. Thielemans, Synthesis of polycaprolactone: a review, Chem. Soc. Rev. 38 (12) (2009) 3484–3504.
[21] C. Vepari, D.L. Kaplan, Silk as a biomaterial, Prog. Polym. Sci. 32 (8–9) (2007) 991–1007.
[22] L.-D. Koh, Y. Cheng, C.-P. Teng, Y.-W. Khin, X.-J. Loh, S.-Y. Tee, M. Low, E. Ye, H.-D. Yu, Y.-W. Zhang, Structures, mechanical properties and applications of silk fibroin materials, Prog. Polym. Sci. 46 (2015) 86–110.
[23] G.M. Nogueira, A.C. Rodas, C.A. Leite, C. Giles, O.Z. Higa, B. Polakiewicz, M.M. Beppu, Preparation and characterization of ethanol-treated silk fibroin dense membranes for biomaterials application using waste silk fibers as raw material, Bioresour. Technol. 101 (21) (2010) 8446–8451.
[24] A. Valipouri, A.A. Gharehaghaji, A. Alirezazadeh, S.A.H. Ravandi, Porosity characterization of biodegradable porous poly (L-lactic acid) electrospun nanofibers, Mater. Res. Express 4 (12) (2017), 125002.
[25] E.J. Chong, T.T. Phan, I.J. Lim, Y.Z. Zhang, B.H. Bay, S. Ramakrishna, C.T. Lim, Evaluation of electrospun PCL/gelatin nanofibrous scaffold for wound healing and layered dermal reconstitution, Acta Biomater. 3 (3) (2007) 321–330.
[26] G. Perumal, S. Pappuru, D. Chakraborty, A.M. Nandkumar, D.K. Chand, M. Doble, Synthesis and characterization of curcumin loaded PLA—hyperbranched polyglycerol electrospun blend for wound dressing applications, Mater. Sci. Eng. C 76 (2017) 1196–1204.
[27] A. Fakhari, C. Berkland, Applications and emerging trends of hyaluronic acid in tissue engineering, as a dermal filler and in osteoarthritis treatment, Acta Biomater. 9 (7) (2013) 7081–7092.
[28] Q. Lu, B. Zhang, M. Li, B. Zuo, D.L. Kaplan, Y. Huang, H. Zhu, Degradation mechanism and control of silk fibroin, Biomacromolecules 12 (4) (2011) 1080–1086.
[29] M. Rottmar, M. Richter, X. Mäder, K. Grieder, K. Nuss, A. Karol, B. von Rechenberg, E. Zimmermann, S. Buser, A. Dobmann, In vitro investigations of a novel wound dressing concept based on biodegradable polyurethane, Sci. Technol. Adv. Mater. 16 (3) (2015), 034606.
[30] C. Turek, F.C. Stintzing, Stability of essential oils: a review, Compr. Rev. Food Sci. Food Saf. 12 (1) (2013) 40–53.
[31] B. Gupta, R. Agarwal, M. Alam, Textile-based Smart Wound Dressings, 2010.
[32] R. Xu, H. Xia, W. He, Z. Li, J. Zhao, B. Liu, Y. Wang, Q. Lei, Y. Kong, Y. Bai, Controlled water vapor transmission rate promotes wound-healing via wound re-epithelialization and contraction enhancement, Sci. Rep. 6 (2016), 24596.
[33] M.F. Jonkman, I. Molenaar, P. Nieuwenhuis, P. Bruin, A.J. Pennings, New method to assess the water vapour permeance of wound coverings, Biomaterials 9 (3) (1988) 263–267.
[34] P.I. Morgado, P.F. Lisboa, M.P. Ribeiro, S.P. Miguel, P.C. Simões, I.J. Correia, A. Aguiar-Ricardo, Poly (vinyl alcohol)/chitosan asymmetrical membranes: highly controlled morphology toward the ideal wound dressing, J. Membr. Sci. 469 (2014) 262–271.
[35] Y. Chen, L. Yan, T. Yuan, Q. Zhang, H. Fan, Asymmetric polyurethane membrane with in situ-generated nano-$TiO_2$ as wound dressing, J. Appl. Polym. Sci. 119 (3) (2011) 1532–1541.
[36] S.M. Oliveira, N.M. Alves, J.F. Mano, Cell interactions with superhydrophilic and superhydrophobic surfaces, J. Adhes. Sci. Technol. 28 (8–9) (2014) 843–863.
[37] Y. Arima, H. Iwata, Effect of wettability and surface functional groups on protein adsorption and cell adhesion using well-defined mixed self-assembled monolayers, Biomaterials 28 (20) (2007) 3074–3082.
[38] Z. Meng, X. Xu, W. Zheng, H. Zhou, L. Li, Y. Zheng, X. Lou, Preparation and characterization of electrospun PLGA/gelatin nanofibers as a potential drug delivery system, Colloids Surf. B: Biointerfaces 84 (1) (2011) 97–102.
[39] T.G. Kim, D.S. Lee, T.G. Park, Controlled protein release from electrospun biodegradable fiber mesh composed of poly(epsilon-caprolactone) and poly(ethylene oxide), Int. J. Pharm. 338 (1–2) (2007) 276–283.
[40] E.-R. Kenawy, F.I. Abdel-Hay, M.H. El-Newehy, G.E. Wnek, Processing of polymer nanofibers through electrospinning as drug delivery systems, Nanomater. Risks Benefits (2009) 247–263 Springer.
[41] S.U. Kumar, I. Matai, P. Dubey, B. Bhushan, A. Sachdev, P. Gopinath, Differentially cross-linkable core–shell nanofibers for tunable delivery of anticancer drugs: synthesis, characterization and their anticancer efficacy, RSC Adv. 4 (72) (2014) 38263–38272.
[42] R. Stern, G. Kogan, M.J. Jedrzejas, L. Soltes, The many ways to cleave hyaluronan, Biotechnol. Adv. 25 (6) (2007) 537–557.
[43] M. Gangwar, M.K. Gautam, S. Ghildiyal, G. Nath, R.K. Goel, *Mallotus philippinensis* Muell. Arg fruit glandular hairs extract promotes wound healing on different wound model in rats, BMC Complement. Altern. Med. 15 (1) (2015) 123.
[44] J. Mastelic, I. Jerkovic, I. Blažević, M. Poljak-Blaži, S. Borović, I. Ivančić-Baće, V. Smrečki, N. Žarković, K. Brčić-Kostic, D. Vikić-Topić, Comparative study on the antioxidant and biological activities of carvacrol, thymol, and eugenol derivatives, J. Agric. Food Chem. 56 (11) (2008) 3989–3996.
[45] M.G. Neuman, R.M. Nanau, L. Oruña-Sanchez, G. Coto, Hyaluronic acid and wound healing, J. Pharm. Pharm. Sci. 18 (1) (2015) 53–60.
[46] K. Kouvidi, A. Berdiaki, D. Nikitovic, P. Katonis, N. Afratis, V.C. Hascall, N.K. Karamanos, G.N. Tzanakakis, Role of receptor for hyaluronan mediated motility (RHAMM) in low molecular weight hyaluronan (LMWHA) mediated fibrosarcoma cell adhesion, J. Biol. Chem. (2011) 38509–38520 (jbc. M111. 275875).
[47] L. Li, Y. Qian, C. Jiang, Y. Lv, W. Liu, L. Zhong, K. Cai, S. Li, L. Yang, The use of hyaluronan to regulate protein adsorption and cell infiltration in nanofibrous scaffolds, Biomaterials 33 (12) (2012) 3428–3445.
[48] H.-S. Joo, M. Otto, Molecular basis of in vivo biofilm formation by bacterial pathogens, Chem. Biol. 19 (12) (2012) 1503–1513.
[49] A.F. Cardona, S.E. Wilson, Skin and soft-tissue infections: a critical review and the role of telavancin in their treatment, Clin. Infect. Dis. 61 (Suppl. 2) (2015) S69–S78.
[50] C. Liolios, O. Gortzi, S. Lalas, J. Tsaknis, I. Chinou, Liposomal incorporation of carvacrol and thymol isolated from the essential oil of *Origanum dictamnus* L. and in vitro antimicrobial activity, Food Chem. 112 (1) (2009) 77–83.
[51] A. Puskarova, M. Buckova, L. Krakova, D. Pangallo, K. Kozics, The antibacterial and antifungal activity of six essential oils and their cyto/genotoxicity to human HEL 12469 cells, Sci. Rep. 7 (1) (2017) 8211.
[52] J.C. Lopez-Romero, H. González-Ríos, A. Borges, M. Simões, Antibacterial effects and mode of action of selected essential oils components against *Escherichia coli* and *Staphylococcus aureus*, Evid. Based Complement. Alternat. Med. 2015 (2015).
[53] D. Trombetta, F. Castelli, M.G. Sarpietro, V. Venuti, M. Cristani, C. Daniele, A. Saija, G. Mazzanti, G. Bisignano, Mechanisms of antibacterial action of three monoterpenes, Antimicrob. Agents Chemother. 49 (6) (2005) 2474–2478.
[54] C. Rota, J. Carraminana, J. Burillo, A. Herrera, In vitro antimicrobial activity of essential oils from aromatic plants against selected foodborne pathogens, J. Food Prot. 67 (6) (2004) 1252–1256.
[55] A.V. Turina, M.V. Nolan, J.A. Zygadlo, M.A. Perillo, Natural terpenes: self-assembly and membrane partitioning, Biophys. Chem. 122 (2) (2006) 101–113.
[56] F. Nazzaro, F. Fratianni, L. De Martino, R. Coppola, V. De Feo, Effect of essential oils on pathogenic bacteria, Pharmaceuticals 6 (12) (2013) 1451–1474.
[57] B.K. Tiwari, V.P. Valdramidis, C.P. O'Donnell, K. Muthukumarappan, P. Bourke, P. Cullen, Application of natural antimicrobials for food preservation, J. Agric. Food Chem. 57 (14) (2009) 5987–6000.
[58] I.M. Helander, H.-L. Alakomi, K. Latva-Kala, T. Mattila-Sandholm, I. Pol, E.J. Smid, L.G. Gorris, A. von Wright, Characterization of the action of selected essential oil components on Gram-negative bacteria, J. Agric. Food Chem. 46 (9) (1998) 3590–3595.